Journal of Solid State Chemistry **168,** 162–168 (2002)
doi:10.1006/jssc.2002.9705

Neutron Diffraction Study of the Ternary Transition Metal Zintl Compound $Ca_{14}MnSb_{11}$

Hyungrak Kim,* Qingzhen Huang,†'‡ Jeffrey W. Lynn,† and Susan M. Kauzlarich*,[1]

Department of Chemistry, University of California, One Shields Ave., Davis, California 95616, USA; †NIST Center for Neutron Research, National Institute of Standards and Technology, Gaithersburg, Maryland 20899-8562; and ‡University of Maryland, College Park, Maryland 20742

Received March 5, 2002; in revised form June 3, 2002; accepted July 16, 2002

The magnetic ordering of the tetragonal $Ca_{14}MnSb_{11}$ compound (space group $I4_1/acd$) has been determined by high-resolution neutron diffraction on powder samples. Neutron data were obtained at temperatures of 1.4, 10, 95 K, and room temperature. Refinement of the magnetic structure reveals a ferromagnetic ordering of Mn magnetic moments lying in the $a-b$ plane below the T_C of 63 K. The low-temperature-ordered magnetic moment on the Mn ion is 3.4(2) μ_B at 1.4 K. The results are confirmed by magnetic susceptibility measurements, which show that the easy magnetization direction of the compound is perpendicular to the *c*-axis and the system orders ferromagnetically at 63 K, in good agreement with neutron diffraction results. A large negative magnetoresistance effect ($\Delta\rho/\rho(H) = -34.4\%$) at the magnetic transition temperature is observed in applied magnetic fields up to 6 T. © 2002 Elsevier Science (USA)

Key Words: **ternary transition metal zintl compound; neutron diffraction; magnetic structure; colossal magnetoresistance; magnetocrystalline anisotropy.**

INTRODUCTION

A large number of new ternary transition Zintl compounds, $A_{14}MnPn_{11}$ (A = alkaline or rare earth metals, Pn = pnictogens), have been synthesized and characterized in recent years (1–7). Since the first discovery of the structure type $Ca_{14}AlSb_{11}$ (8), the properties of the new transition metal Zintl phases have attracted a great deal of attention because of their interesting magnetic and magnetotransport behaviors. From the point of view of Zintl phases, this structure type is electronically positioned at the borderline between the intermetallic and insulating valence compounds (9). A detailed electrical resistivity study shows that the compounds can be categorized as either a narrow gap semiconductor or a metal depending on the pnictogen element (3, 4, 10) and the transport properties are closely coupled to the magnetic ordering of the compounds (11–13).

The $A_{14}MnPn_{11}$ compounds crystallize in a body-centered tetragonal unit cell in the space group $I4_1/acd$ with eight formula units (208 atoms). A formula unit consists of 14 interstitial A^{2+}, 4 isolated Pn^{3-}, a distorted $MnPn_4^{9-}$ tetrahedron, and a Pn_3^{7-} linear anion. The structure can be described as a combination of free metal cations and anionic units, as found in many other ternary Zintl phases (14). There are four crystallographically inequivalent sites of both A and Pn. All the Mn sites in the crystal structure are equivalent and approximately 10 Å from their nearest neighbors. In this simple model, Mn is expected to be Mn^{3+}.

The unexpectedly high magnetic ordering temperature of the well-separated Mn moments has been explained by the Rudermann–Kittel–Kasuya–Yosida (RKKY) interaction (15–17). The trend of the exchange interaction strength in the alkaline earth analogs, $A_{14}MnPn_{11}$ (A = Ca, Sr, Ba; Pn = Sb, Bi), is understood according to the simple free electron isotropic RKKY theory (4). A study of pressure-induced magnetic ordering in $Sr_{14}MnAs_{11}$ (10) provides further support for this model, indicating that the magnetic interaction between the localized moments is mediated by conduction electrons. The study also shows that the size of the metal cation and pnictogen element has a key role in determining the electrical and magnetic properties of the compound by changing the overlap of the anion wave functions resulting in a modified energy band gap. The continuous efforts to elucidate the magnetic properties of the compounds have been expanded to more complex systems, such as the rare-earth transition metal ternaries $Eu_{14}MnPn_{11}$ (6, 18, 19), $Yb_{14}MnPn_{11}$(5,11), and the pseudo-ternaries $Eu_{14-x}A_xMnSb_{11}$ (A = Ca, Sr, Ba, Yb, Gd) (7, 20, 21).

Although there have been a large number of studies of this structure type, their magnetic structures have never been determined. The colossal magnetoresistance observed

---

[1] To whom correspondence should be addressed. Fax: 530-752-8995. E-mail: smkauzlarich@ucdavis.edu.

0022-4596/02 $35.00

in many of these compounds provides the motivation along with recent theoretical calculations (24) to explore the magnetic structure of these compounds. The present paper reports the first investigation of the magnetic structure of $Ca_{14}MnSb_{11}$ by high-resolution neutron powder diffraction. $Ca_{14}MnSb_{11}$ was chosen since it contains only Mn as the magnetic ion, and appears to be a simple ferromagnet with a relatively high transition temperature, 63 K (4). We also include new single crystal magnetic and magnetotransport properties.

EXPERIMENTAL SECTION

Synthesis

Ca pieces (J. Matthey, 99.99%) and Sb (J. Matthey, 99.9999%) were used as received. Mn flakes (J. Matthey, 99.98%) were first cleaned in a 5% HNO_3/CH_3OH solution, transferred into a nitrogen-filled drybox and ground into a powder. A stoichiometric mixture of the elements was loaded into a clean tantalum tube with a sealed end and subsequently sealed in an argon-filled arc welder. Ta tubes were cleaned prior to arc welding with 20% HF, 25% HNO_3, and 55% H_2SO_4 solution. The sealed Ta tube was further sealed in a fused silica tube under $\frac{1}{5}$ atmosphere-purified argon. A total of six reactions, each targeting 1 g of final product, were prepared. Highly reflective polycrystalline pieces and single crystal needles (2–3 mm) were obtained by heating the mixtures in a two-zone furnace with $T_{high} = 1000°C$ and $T_{low} = 950°C$ for 10 days. All reactants were mixed together and ground into a fine powder sample in a nitrogen-filled drybox with water levels less than 1 ppm.

Neutron Powder Diffraction

The neutron powder diffraction experiments were carried out at the NIST Center for Neutron Research. The neutron powder diffraction profile was obtained in the BT-1 high-resolution powder diffractometer. The sample was sealed in a vanadium cylindrical holder and loaded into a pumped helium top-loading cryostat. A Ge (311) monochromator was employed to produce a neutron beam of the wavelength of 2.0784 Å. The longer wavelength is particularly useful for the study of magnetic structures, providing more intensity as well as better resolution in the low 2θ angle. The diffraction intensity data were collected in the 2θ range of 5–165° with steps of 0.05° at the three different temperatures, 1.4, 10, and 95 K. The temperature-dependent magnetic diffraction measurements were performed on the BT-2 triple axis spectrometer, employing a pyrolytic graphite monochromator with a wavelength of 2.359 Å. The magnetic intensity was measured at an angle of 16.65° while cooling the sample from 80 to 1.4 K in steps of 1 K, to determine the temperature dependence of the magnetic order parameter. A detailed investigation of the neutron diffraction data was also carried out in the 2θ range of 14.5–19° with $10'$ collimation to achieve high resolution on the BT-2 spectrometer. The (0,2,0) and (1,1,2) peaks could then be split, and the temperature dependences of two magnetic peaks were compared in order to ascertain that they exhibit the same temperature dependence. GSAS program (22) was employed in the crystal and magnetic structure refinements.

Magnetic Susceptibility and Transport Measurements

DC magnetization was measured using a quantum design MPMS superconducting quantum interference device (SQUID) magnetometer with a 7 T superconducting magnet. The data were collected and analyzed with the magnetic property measurement system (MPMS) software (23) provided by Quantum Design. The needle crystal was placed in the parallel direction to the applied magnetic field first and switched to the perpendicular direction to determine the magnetocrystalline anisotropy of the compound. For single crystal magnetic measurements, the DC magnetization measurements were performed in the temperature range of 2–80 K by changing the applied field from 200 to 5000 Oe. Powdered samples were prepared in a drybox by loading 65 mg into a gel-capsule and suspending it in a low background sample holder. Zero-field cooled (ZFC) measurements were made by cooling the sample in zero field down to 2 K and then applying a field and measuring the magnetization while warming from 2 to 300 K. Field-cooled measurements were made on the sample with an applied field from 300 to 2 K. The hysteresis data were taken after the temperature-dependent magnetization measurements, but in order to remove the remnant field or magnetization, the sample was brought to room temperature and cooled to the corresponding temperature in order to perform the hysteresis measurement. Magnetoresistance measurements of the $Ca_{14}MnSb_{11}$ compound were performed on a needle-shaped single crystal with dimensions of $0.05 \times 0.05 \times 1.2\,mm^3$ using a standard four-probe method. Pt leads were attached with silver paint. A constant current (0.1 mA) was applied to the sample along the crystal *c*-axis through the two outer leads (Keithley Model 224 current source) and the voltage was measured across the two inner leads (Keithley Model 196 nanovoltmeter).

RESULTS AND DISCUSSION

Figure 1 shows the temperature-dependent magnetization of the powder sample of $Ca_{14}MnSb_{11}$, which has been used for the neutron diffraction experiment. The magnetic measurement was carried out in an applied magnetic field

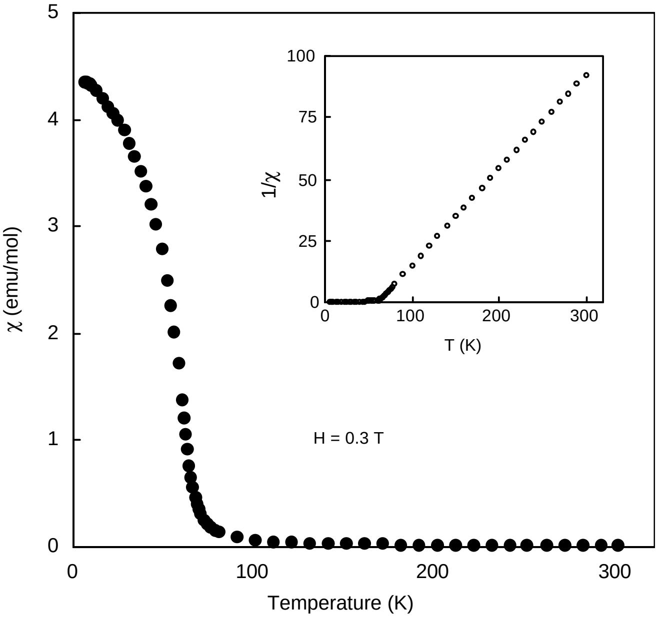

FIG. 1. Field-dependent magnetic susceptibility of polycrystalline $Ca_{14}MnSb_{11}$ measured at $H = 0.3\,T$. The inset shows the plot of inverse magnetic susceptibility as a function of temperature.

of 3000 Oe and the inset shows the inverse magnetic susceptibility as a function of temperature. The compound displays simple paramagnetic behavior at higher temperatures and undergoes a ferromagnetic transition at 63 K. The high-temperature paramagnetic data (80–300 K) were fit to a modified Curie–Weiss law ($\chi = C/(T - \theta) + \chi_0$) and the following parameters were obtained: $\chi_0 = 0.00052(5)$ emu/mol; $C = 2.47(1)$; and $\theta = 62.5(1)$ K. The effective moment per formula unit is $4.44(2)\,\mu_B$ calculated from the Curie constant. This is slightly less than the expected value for $Mn^{3+}(d^4)$ of $4.90\,\mu_B$.

Figure 2(a) presents a hysteresis loop of the powder sample at 2 K and it shows the characteristic curve of a ferromagnetic material with a small coercive field. Several field-dependent magnetization curves at different temperatures are included in Fig. 2(b) for comparison. As the temperature decreases below 60 K, the compound readily approaches its saturation magnetization with a low applied magnetic field and shows a maximum value $2.77\,\mu_B$ at 2 K under 6 T. The saturation moment obtained here is consistent with the previous result of $Ca_{14}MnSb_{11}$ (4) which also showed a value smaller than the $4\,\mu_B$ that one would expect for four unpaired spins. The deviation from $4\,\mu_B$ has been attributed to the polarization of the conduction electrons and has also been found in many other semimetallic Sb- or Bi-analogs (3, 4) of this structure-type compound. Recent theoretical calculations for $Ca_{14}MnBi_{11}$ and $Ba_{14}MnBi_{11}$ (25) suggest that Mn is Mn^{2+} (d^5) with a hole residing on the Bi atoms in the $MnBi_4$ tetrahedron. The polarized hole is distributed over the four Bi atoms and partially compensates for the Mn^{2+} five unpaired spins, giving rise to an overall moment that is consistent with the Mn^{3+} model.

Figure 3 shows the magnetization data of a single crystal as a function of temperature. The needle-shaped crystal was placed with its crystal *c*-axis parallel (open circles) to the applied field and then rotated perpendicular (black circles) to the applied field to determine the magnetocrystalline anisotropy in the compound. The magnetization in the perpendicular orientation shows much larger values than the one in parallel orientation, which indicates that the easy magnetization axis of the compound lies in the *ab* plane.

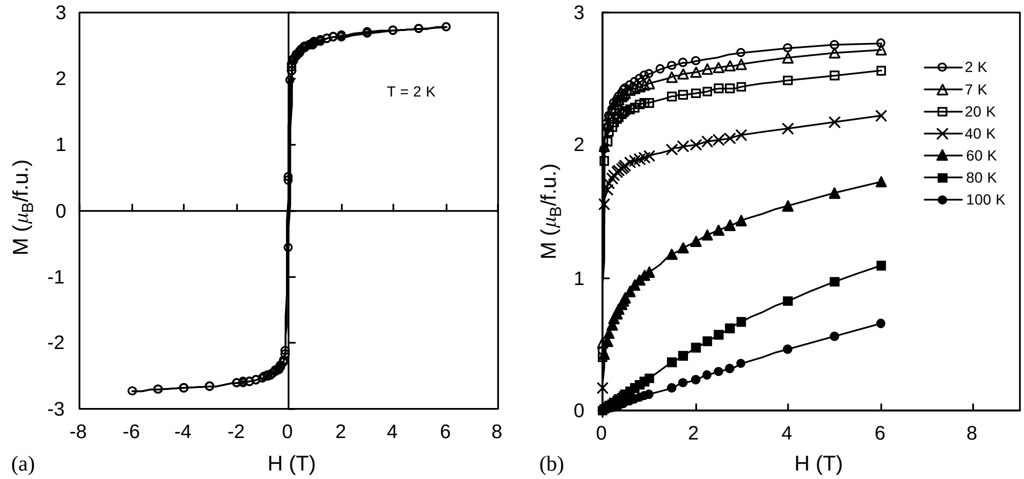

FIG. 2. (a) Hysteresis loop of polycrystalline $Ca_{14}MnSb_{11}$ measured at 2 K, (b) Field-dependent magnetization of polycrystalline $Ca_{14}MnSb_{11}$ measured at various temperatures.

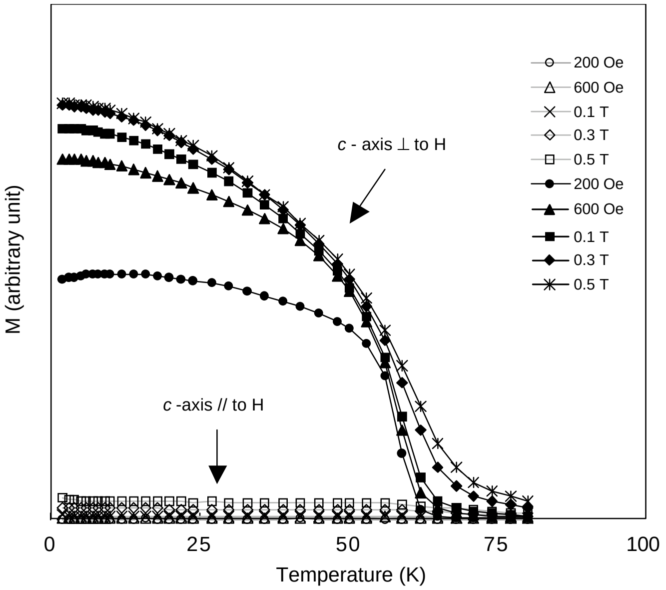

FIG. 3. Anisotropic magnetization of a single crystal $Ca_{14}MnSb_{11}$ as a function of temperature.

Neutron powder diffraction data were obtained on the same sample described above. Most of the Bragg reflections of the $Ca_{14}MnSb_{11}$ powder sample measured on the BT-1 diffractometer could be indexed with the tetragonal space group $I4_1/acd$, determined in the single-crystal X-ray study (4). Some additional peaks were identified to be $CaMnSb_2$ phase ($\sim 20\%$) and those peaks were excluded in the final refinement. As the temperature decreases below the magnetic transition temperature ($T_C = 63\,K$), the intensities of several diffraction peaks at lower angle increase significantly. As shown in Fig. 4(a), after fitting with the nuclear structure based on the X-ray results, extra intensities were found to be superposed on the (2,0,0), (1,1,2), (2,0,0), (0,0,4), (1,3,2), and (2,0,4) reflections. To investigate the nature of these intensities, we performed higher statistical neutron powder diffraction experiments on the same powder sample below and above the magnetic transition temperature on the BT-2 spectrometer. The diffraction intensity data were collected in the 2θ range of 3–50° with steps of 0.10° for 2 min/point at the two different temperatures, 1.4 and 80 K. By subtracting (24) the scattering data observed above the transition temperature from the low-temperature data, the magnetic diffraction peaks in the low 2θ range can be discerned. Figure 4(b) shows the fit to the data using a ferromagnetic model with the Mn moments in the *ab* plane.

The temperature dependence of the magnetic intensity for the strongest magnetic peak is shown in Fig. 5. These data were collected at the 2θ angle of 16.65°, which result from the overlap of the (0,2,0) and (1,1,2) peaks. The solid curve is a fit to the Brillouin function, and we obtain an ordering temperature of 62.9(9) K, which is in very good agreement with the paramagnetic Curie temperature, 62.5(1) K, from the temperature-dependent magnetization measurement of the same powder sample. These results demonstrate that the extra intensities observed at lower angle in the BT1 data are magnetic in origin. A ferromagnetic model with ordered Mn moments in the *ab* plane provides a very good description of the magnetic intensities, as shown in Fig. 4(b). The value of the ordered moment at low temperatures obtained from the fit is $3.4(2)\,\mu_B$. This is in excellent agreement with the moment $2.77\,\mu_B$ determined in the magnetic measurements, once the impurity content of 20% is taken into account. The final structural parameters, selected interatomic distances, and angles obtained from the refinements using GSAS program are given in Table 1.

Recent theoretical work (25) for the Bi compounds, $Ca_{14}MnBi_{11}$ and $Ba_{14}MnBi_{11}$, suggests a different model for magnetization and consequently, a different magnetic moment for the Mn atom. As mentioned previously, this

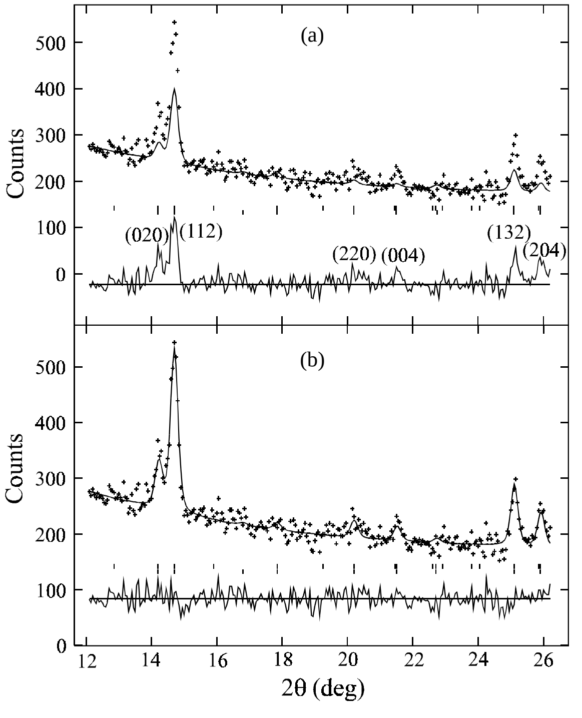

FIG. 4. Portion of the observed (crosses) and calculated (solid line) neutron powder diffraction pattern of Ca14MnSb11 at 1.4 K. The differences between observed and calculated profiles are given as solid curves in the bottom of the figures. Vertical lines correspond to Bragg peak positions for nuclear (bottom) and magnetic (top) reflections. (a) Fitted by nuclear structure only. The differences show the residual intensities contributed from the ferromagnetic ordering. (b) Both nuclear and magnetic structure are considered in the calculation. A ferromagnetic model with the Mn moments in the *ab* plane gives a good fit to the observed magnetic intensities.

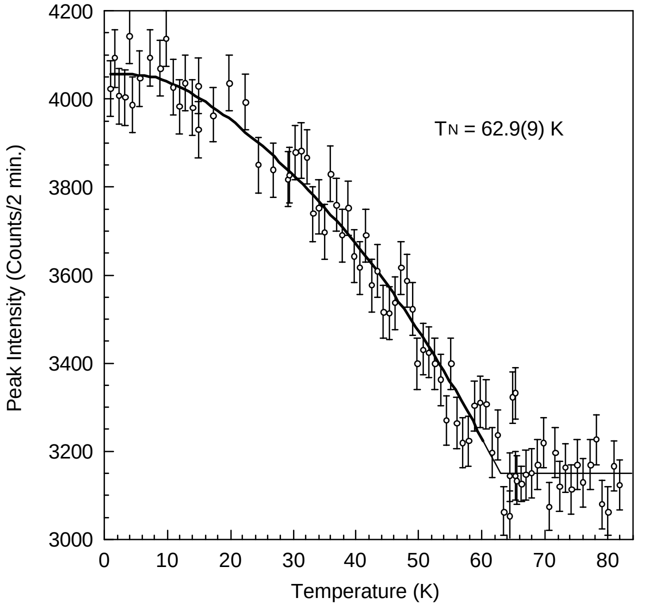

FIG. 5. Temperature dependence of the intensity of the magnetic peak collected at the 2θ angle of 16.65°, which results from the overlap of the (0,2,0) and (1,1,2) peaks. The solid curve is a fit to a Brillouin function.

study shows that there is a polarized hole residing in the $MnBi_4$ tetrahedral unit and it partially compensates the high spin d^5 Mn moment leaving a net spin $4\,\mu_B$, which is close to the experimental value. The theoretical model is similar to the transfer of moment (and charge) via chemical bonding, which has been an interesting "magnetic form factor" subject (26) for many years. We performed a refinement using this model in order to see any magnetic moment on Sb(2) site, but it is not observable from our powder data. Neutron diffraction on a single crystal will be necessary to further explore this model.

Figure 6 shows the $MnSb_4$ tetrahedra arrangement in the structure of $Ca_{14}MnSb_{11}$; the other nonmagnetic elements are not shown for clarity. The Mn atoms are located in the center of slightly distorted $MnSb_4$ tetrahedra in which the Mn–Sb(2) distance is 2.76 Å and Sb(2)–Mn–Sb(2) angles are 106.5(2)° and 115.6(4)°. Each Mn has eight nearest neighbors (~10.03 Å apart) and four second nearest neighbors (~11.8 Å). All Mn atoms have magnetic moments ordered ferromagnetically in the *ab* plane (parallel to the *b*-axis shown by arrows in Fig. 6 with magnitudes ($3.4(2)\,\mu_B$ at 1.4 K) consistent with Mn^{3+}. The

TABLE 1
Structural Parameters and Selected Interatomic Distances (Å) and Angles (deg) for $Ca_{14}MnSb_{11}$ at 1.4 K (First Line) and 95 K (Second Line)

Atom	Site	*x*	*y*	*z*	*B* (Å)	Moment (μ_B)
Ca(1)	32*g*	−0.0415(5)	−0.0704(6)	0.8260(5)	0.5(1)	
		−0.0419(7)	−0.0688(9)	0.8261(7)	0.6(1)	
Ca(2)	32*g*	−0.0230(5)	0.1255(7)	0.0077(4)	0.5(1)	
		−0.0235(8)	0.1274(9)	0.0077(6)	0.6(1)	
Ca(3)	16*e*	0.3548(9)	0	$\frac{1}{4}$	0.5(1)	
		0.3568(12)	0	$\frac{1}{4}$	0.6(1)	
Ca(4)	32*g*	0.1779(6)	0.4078(5)	0.8426(6)	0.5(1)	
		0.1804(8)	0.4075(7)	0.8428(8)	0.6(1)	
Mn	8*a*	0	$\frac{1}{4}$	$\frac{7}{8}$	0.6(2)	3.4(2) (in *ab* plane)
		0	$\frac{1}{4}$	$\frac{7}{8}$	0.7(2)	
Sb(1)	16*f*	0.1393(5)	0.3892(5)	$\frac{1}{8}$	0.5(2)	
		0.1378(8)	0.3877(8)	$\frac{1}{8}$	0.6(2)	
Sb(2)	32*g*	0.0043(5)	0.1101(6)	0.8086(3)	0.5(2)	
		0.0044(8)	0.1122(9)	0.8078(5)	0.6(2)	
Sb(3)	32*g*	0.8704(5)	0.9746(5)	0.9558(4)	0.5(2)	
		0.8708(7)	0.9742(8)	0.9569(6)	0.6(2)	
Sb(4)	8*b*	0	$\frac{1}{4}$	$\frac{1}{8}$	0.5(2)	
		0	$\frac{1}{4}$	$\frac{1}{8}$	0.6(2)	
$MnSb_4$ tetrahedron						
Mn–Sb(2) × 4		2.76(1)	Sb(2)–Sb(2) × 2		4.68(2)	(in tetrahedron)
		2.75(1)			4.61(2)	
Sb(2)–Mn–Sb(2) × 4		106.5(2)	Sb(2)–Sb(2) × 4		4.43(2)	(in tetrahedron)
		107.2(3)			4.39(2)	
Sb(2)–Mn–Sb(2) × 2		115.6(4)	Sb(2)–Sb(2)		4.51(2)	(between tetrahedron)
		114.1(5)			4.55(3)	

Note. Space group: $I4_1/acd$ (#142). $a = 16.710(1), c = 22.205(2)$ Å, $z = 8$, $R_p = 4.80\%$, $R_{wp} = 6.09\%$, $\chi^2 = 1.421$. 16.716(3), 22.217(4) 8. 7.27%, 8.83% 0.9683. The neutron scattering amplitudes used in the refinement are 0.490, −0.373, and 0.564×10^{-12} cm for Ca, Mn, and Sb, respectively.

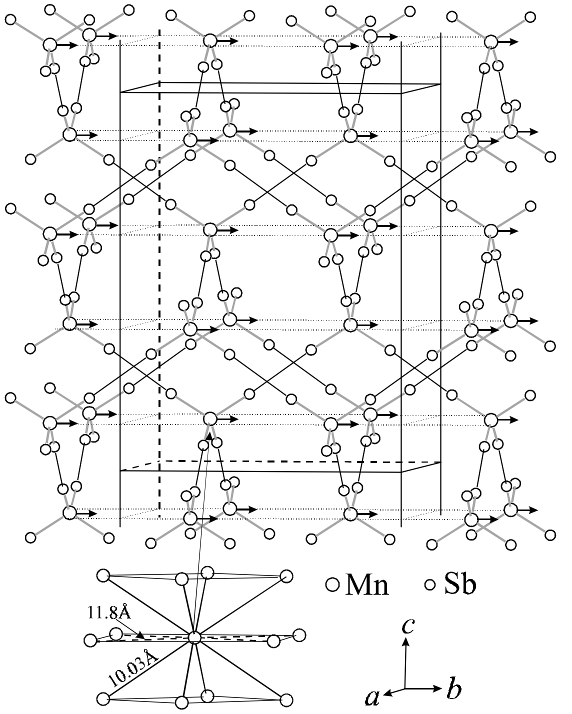

FIG. 6. View of the $MnSb_4$ tetrahedra arrangement in the $Ca_{14}MnSb_{11}$ structure. The arrows show one of the possible Mn moment directions (*b*-axis) in the *ab* plane.

moment, along with the distortion of the tetrahedron, supports a simple model of Mn^{3+}.

There was an unusual decrease of magnetization for both the powder and single-crystal samples when decreasing temperature below 10 K at low magnetic field, as shown in the low-temperature region of Figs. 1 and 3. One of the possible causes of the decrease might be a competition between two or more magnetic sublattices which may have a different magnetization process as a function of temperature. We expect that the higher resolution neutron diffraction experiment would be able to reveal the possible discrepancy in their temperature dependencies of the (0,2,0) and (1,1,2) peaks. A set of diffraction data on BT-2 in the 2θ range of 14.5–19° using the $10'$–$10'$ collimation before and after the monochromator was collected. Complete scans were performed at 1.4, 10, 25, 40, and 80 K and Fig. 7 shows subtraction results of the separated (0,2,0) and (1,1,2) peaks. The three different temperatures, 1.4, 10, and 80 K in Fig. 7 were chosen based on consideration of the temperature-dependent magnetization results of $Ca_{14}MnSb_{11}$ as well as the order parameter measurement just presented. As shown in Fig. 7, there is no significant difference in their magnetic scattering intensities. Thus, we conclude that the decrease of magnetization below 10 K at low magnetic field is caused by the magnetocrystalline anisotropy of the compound, which was observed in Fig. 3.

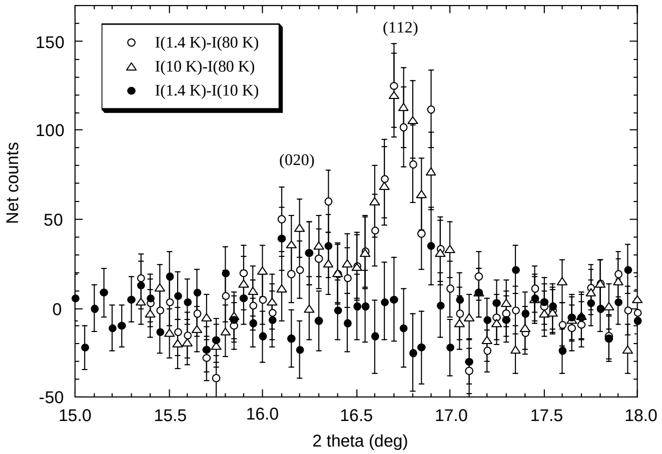

FIG. 7. Subtraction results for the (0,2,0) and (1,1,2) magnetic peaks at two different temperatures.

Figure 8 presents the experimental results of the temperature-dependent resistivity of the $Ca_{14}MnSb_{11}$ compound in various magnetic fields. In the high-temperature range the compound shows semiconducting behavior with $\rho_{RT} = 6.29 \times 10^{-3}\,\Omega\,\mathrm{cm}$, but as the temperature decreases below the magnetic transition temperature the compound exhibits metallic behavior. The transition from paramagnetic semiconducting to ferromagnetic metallic state is broad compared to the ternary rare-earth transition metal compounds of the same structure type (6, 7, 19). Figure 9 shows a plot of the magnetoresistance ratio ($\mathrm{MR} = [(\rho(H) - \rho(0))/\rho(H)] \times 100\%$) as a function of temperature. The ratios have a similar order-of-magnitude as $Eu_{14}MnSb_{11}$ (6) and peak near the transition

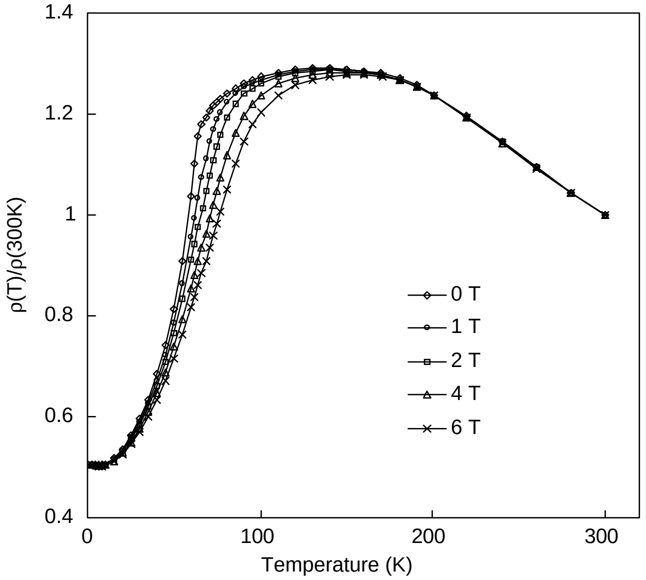

FIG. 8. Electrical resistivity versus temperature of a $Ca_{14}MnSb_{11}$ single crystal for various magnetic fields.

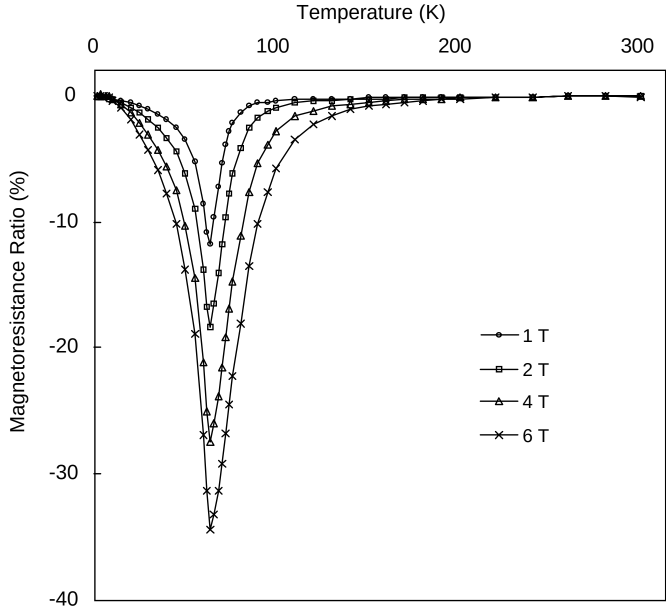

FIG. 9. Magnetoresistance ratio versus temperature of a $Ca_{14}MnSb_{11}$ single crystal for various applied magnetic fields.

temperature from semiconducting to metallic state at 6 T. There is good agreement between the transition temperature of MR plot, 64 K and the paramagnetic Curie temperature of the compound, 63 K. It indicates a close relationship between the electrical and magnetic properties of the compound.

The negative colossal magnetoresistance, CMR, effect of $Ca_{14}MnSb_{11}$ can also be understood by the reduction in spin disorder scattering model which was proposed in the previous studies of $Eu_{14}MnPn_{11}$ and $Yb_{14}MnPn_{11}$ (Pn = Sb, Bi) (6, 11, 12). The conduction electrons, mainly from the Mn 4*s* band in this case, will experience a variable spin scattering from the localized magnetic moments of the Mn *d*-electrons depending on their relative spin orientations and, consequently, the resistivity will be both temperature and field dependent. The compound experiences a large change of electrical resistance decided by the relative spin orientations because most of the Sb- and Bi-analogs with the $Ca_{14}AlSb_{11}$ structure have a nearly zero band gap and low density polarized conduction electrons mediating the long-range magnetic ordering by the RKKY mechanism.

ACKNOWLEDGMENTS

We thank the National Science Foundation (DMR 9803074, 0120990) for funding. We thank R. N. Shelton for use of the SQUID magnetometer, P. Klavins for useful discussion. The identification of any commercial product or trade name does not imply endorsement or recommendation by the National Institute of Standards and Technology.

REFERENCES

1. S. M. Kauzlarich, T. Y. Kuromoto, and M. M. Olmstead, *J. Am. Chem. Soc.* **111,** 8041 (1989).
2. D. J. Webb, T. Y. Kuromoto, and S. M. Kauzlarich, *J. Magn. Magn. Mater.* **98,** 71 (1991).
3. T. Y. Kuromoto, S. M. Kauzlarich, and D. Webb, *J. Chem. Mater.* **4,** 435 (1992).
4. A. Rehr, T. Y. Kuromoto, S. M. Kauzlarich, J. D. Castillo, and D. J. Webb, *Chem. Mater.* **6,** 93 (1994).
5. J. Y. Chan, M. M. Olmstead, and S. M. Kauzlarich, *Chem. Mater.* **10,** 3583 (1998).
6. J. Y. Chan, S. M. Kauzlarich, P. Klavins, R. N. Shelton, and D. J. Webb, *Chem. Mater.* **9,** 3132 (1997).
7. H. Kim, J. Y. Chan, M. M. Olmstead, P. Klavins, D. J. Webb, and S. M. Kauzlarich, *Chem. Mater.* **14,** 206 (2002).
8. G. Cordier, H. Schäfer, and M. Stelter, *Z. Anorg. Allg. Chem.* **519,** 183 (1984).
9. S. M. Kauzlarich, *in*: Chemistry "Structure, and Bonding of Zintl Phases and Ions," (S. M. Kauzlarich, Ed.), pp. 245–274. VCH Publishers, New York, 1996.
10. J. D. Castillo, D. J. Webb, S. M. Kauzlarich, and T. Y. Kuromoto, *Phys. Rev. B* **47,** 4849 (1993).
11. I. R. Fisher, T. A. Wiener, S. L. Bud'ko, P. C. Canfield, J. Y. Chan, and S. M. Kauzlarich, *Phys. Rev. B* **59,** 13829 (1999).
12. J. Y. Chan, S. M. Kauzlarich, P. Klavins, R. N. Shelton, and D. J. Webb, *Phys. Rev. B* **57,** R8103 (1998).
13. D. J. Webb, R. Cohen, P. Klavins, R. N. Shelton, J. Y. Chan, and S. M. Kauzlarich, *J. Appl. Phys.* **83,** 7192 (1998).
14. E. G. C. Brigitte, *in*: "Structural Patterns of Homo- and Heteronuclear Anions in Zintl Phases and Related Intermetallic Compounds and Concepts for Their Interpretation." (G. C. Brigitte Eisenmann, Ed.), pp. 245–274. VCH Publishers, New York, 1996.
15. M. A. Ruderman, *Phys. Rev.* **96,** 99 (1954).
16. T. Kasuya, *Prog. Theor. Phys.* **16,** 45 (1956).
17. K. Yosida, *Phys. Rev.* **106,** 893 (1957).
18. J. Y. Chan, M. E. Wang, A. Rehr, S. M. Kauzlarich, and D. J. Webb, *Chem. Mater.* **9,** 2132 (1997).
19. A. C. Payne, M. M. Olmstead, S. M. Kauzlarich, and D. J. Webb, *Chem. Mater.* **13,** 1398 (2001).
20. J. Y. Chan, S. M. Kauzlarich, P. Klavins, J.-Z. Liu, R. N. Shelton, and D. J. Webb, *Phys. Rev. B* **61,** 459 (2000).
21. H. Kim, P. Klavins, and S. M. Kauzlarich, *Chem. Mater.* **14,** 2308 (2002).
22. A. C. Larson and R. B. Von Dreele, "General Structure Analysis System." Report no. LAUR086-748, Los Alamos National Laboratory, NM, 1994.
23. *MPMS XL7*, Quantum Design Inc., San Diego, CA 92121.
24. H. Zhang, J. W. Lynn, W.-H. Li. T. W. Clinton, and D. E. Morris, *Phys. Rev. B* **41,** 11229 (1990).
25. D. Sanchez-Portal, R. M. Martin, S. M. Kauzlarich, and W. E. Pickett. *Phys. Rev. B* **65,** 144414 (2002).
26. J. W. Lynn, G. Shirane, and M. Blume, *Phys. Rev. Lett.* **37,** 154 (1976).